Authors for correspondence:
Raphaël Sarfati
e-mail: raphael.sarfati@colorado.edu
Orit Peleg
e-mail: orit.peleg@colorado.edu

THE ROYAL SOCIETY
PUBLISHING

Spatio-temporal reconstruction of emergent flash synchronization in firefly swarms via stereoscopic 360-degree cameras

Raphaël Sarfati[1], Julie C. Hayes[1], Élie Sarfati[2] and Orit Peleg[1,3,4]

[1]BioFrontiers Institute, University of Colorado Boulder, Boulder, CO, USA
[2]Rubika Supinfogame, Valenciennes, France
[3]Computer Science, University of Colorado Boulder, Boulder, CO, USA
[4]Santa Fe Institute, Santa Fe, NM, USA

RS, 0000-0003-4944-0632; JCH, 0000-0002-4363-3559; OP, 0000-0001-9481-7967

During mating season, males of synchronous firefly species flash in unison within swarms of thousands of individuals. These strongly correlated collective displays have inspired numerous mathematical models to explain how global synchronous patterns emerge from local interactions. Yet, experimental data to validate these models remain sparse. To address this gap, we develop a method for three-dimensional tracking of firefly flashes, using a stereoscopic set-up of 360-degree cameras. We apply this method to record flashing displays of the North American synchronous species *Photinus carolinus* in its natural habitat as well as within controlled environments, and obtain the three-dimensional reconstruction of flash occurrences in the swarm. Our results show that even a small number of interacting males synchronize their flashes; however, periodic flash bursts only occur in groups larger than 15 males. Moreover, flash occurrences are correlated over several metres, indicating long-range interactions. While this suggests emergent collective behaviour and cooperation, we identify distinct individual trajectories that hint at additional competitive mechanisms. These reveal possible behavioural differentiation with early flashers being more mobile and flashing longer than late followers. Our experimental technique is inexpensive and easily implemented. It is extensible to tracking light communication in various firefly species and flight trajectories in other insect swarms.

1. Introduction

Firefly flashes are more than a mere midsummer night's wonder: they express a sophisticated social behaviour characterized by male courtship and female mate choice [1]. Firefly swarms are mass-mating events that contain purposeful internal dynamics [2]. Importantly, fireflies offer a rare glimpse into insect communication, as their broadcasting signals, consisting of intermittent and periodic flash patterns, are readily traceable even in congested groups. Therefore, it is possible to separate movement from communication, unlike in other insect swarms where trajectories are a proxy for social interactions [3,4]. During mating season, male fireflies advertise themselves to stationary females on the ground by flashing their species-specific patterns to be identified as potential mates [2,5]. Flash production is a voluntary action, resulting from the well-timed release of the neurotransmitter octopamine triggering the luciferin–luciferase chemical reaction in the insect's lantern [6].

In certain species, males flash synchronously in unison within swarms of tens of thousands of individuals [7]. This phenomenon, often reported in Southeast
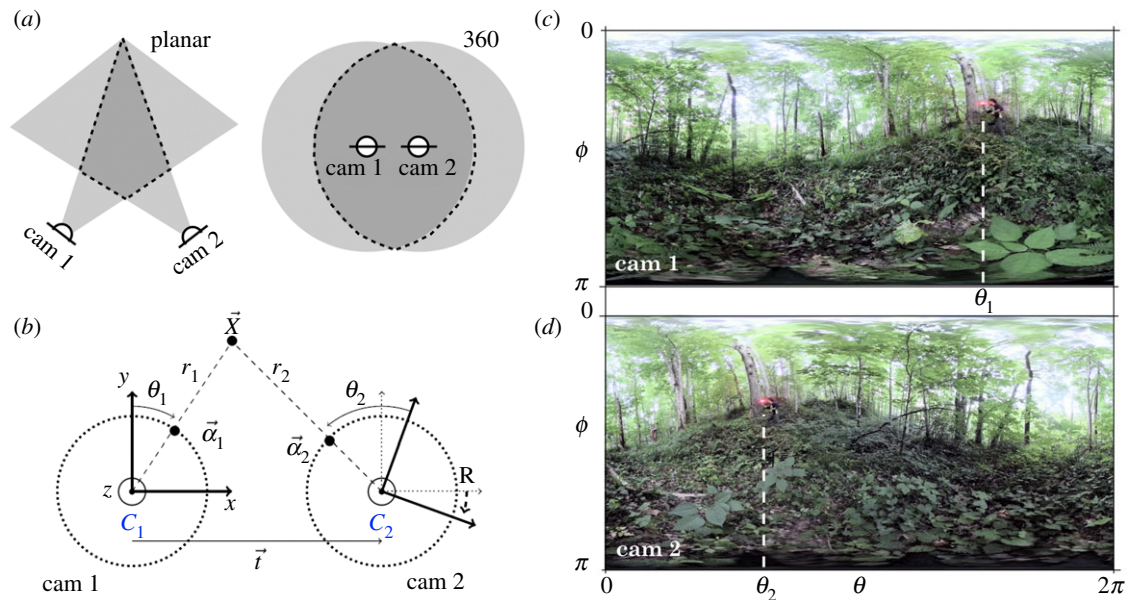
Figure 1. Stereoscopic vision using two 360-cameras. (*a*) Compared with stereoscopic vision using planar cameras, for which the intersection of the FOVs is a cone-like shape (left), 360-cameras positioned close to each other have a sphere-like FOV overlap (right). (*b*) Schematic of the principles of 360 stereo reconstruction, showing the position *t* and orientation **R** of C_2 relative to C_1, and the projections of the world point *X* in the FOV of each camera. For simplicity, the schematic assumes only a rotation around the z-axis, $\mathbf{R} = \mathbf{R_z}(\psi_z)$. (*c,d*) To illustrate, FOVs in (*c*) C_1 and (*d*) C_2 in equirectangular form. The horizontal coordinate maps onto the polar angle θ between 0 and 2π, and the vertical coordinate maps onto the azimuthal angle ϕ between 0 and π (top to bottom). The same red dot, representing *X*, is seen at different (θ, ϕ) positions in C_1 and C_2.

Asia, was first studied by Buck & Buck [8,9]. In North America, the well-studied colony of synchronous species *Photinus carolinus* in the Great Smoky Mountains National Park (GSMNP) mates for 10–15 days in early June, a phenomenon that has attracted tourists and scientists alike for many years [10].

The collective flashing displays of *P. carolinus* have been described in detail, notably by Copeland & Moiseff [11,12], who showed that males flash synchronously every $T_f \simeq 0.5$ s, for bursts of a few seconds, and then collectively stop for a few seconds, leaving their environment completely dark. Flash bursts repeat every $T_b \simeq 12-14$ s for up to 3 h after sunset and are believed to provide an opportunity for females, located close to the ground, to respond outside of visual clutter [13]. As a landmark of synchronization in nature, these displays have inspired various mathematical models to explain how a number of coupled oscillators might find themselves synchronized if given enough time [14,15]. As illustrated by these models, a comprehensive understanding of firefly collective behaviour requires not only temporal but also spatial information about flash occurrences, which has been lacking until now. To address this gap, we captured stereoscopic footage of *P. carolinus* flashing displays in GSMNP in order to obtain three-dimensional reconstructions of flashing swarms.

Traditionally, stereoscopic set-ups have used regular (planar) cameras for the three-dimensional tracking of flocking or swarming animals, such as mosquitoes [3], midges [4,16,17] or birds [18–22], which has provided considerable insights into the mechanisms involved in collective dynamics, for example the structure of interactions [17,19,23] or propagation of information [18,22]. Over the past few years, however, 360-degree cameras (or 360-cameras) have started to be used widely, notably in computer vision [24]. These cameras stitch together multiple fields of view (FOVs) from complementary wide-angle objectives in order to provide a full spherical image. To our knowledge, 360-cameras have not previously been used in the study of swarms and flocks but potentially offer complementing advantages to

traditional techniques. Indeed, while the cone-like overlap between two planar cameras' FOVs is well suited to small swarms or distant flocks, it suffers from significant limitations for large or extended groups such as firefly swarms, as cameras need to be placed outside the collective dynamics and can only capture a sliver of the action (figure 1*a*). By contrast, 360-degree cameras can be placed directly within a swarm of interest, and present a FOV overlap that is more isotropic (figure 1*a*). For firefly swarms, this even enables the recording of collective male displays from the perspective of a stationary female on the ground.

Here, we present a general framework for three-dimensional reconstruction using a pair of 360-cameras, and demonstrate its implementation for the analysis of firefly swarms' internal dynamics, in particular flight patterns and spatio-temporal correlations. This paper consists of three main parts. The next section presents the theory behind the three-dimensional reconstruction technique and its practical implementation, and may be useful to experimentalists for the study of fireflies and other insect swarms. Our Matlab code is provided in the electronic supplementary material, S1.1. The Results section reports findings relative to the behaviour of *P. carolinus* fireflies, and may be of interest to biologists, entomologists, physicists and even the general public. In the following section, we detail some of the advantages and limitations of our experimental technique, and outline possible applications based on the data presented. We also provide with this paper a standalone FireflyNavigator software tool for the reader to interactively navigate reconstructed firefly swarms and visualize trajectories (electronic supplementary material, S1.2).

2. Methods: three-dimensional reconstruction via pairs of 360-degree cameras

Stereoscopic vision uses image projections from two distinct perspectives to triangulate the positions of world

points in three dimensions. Below, we introduce the model underlying stereoscopic reconstruction from pairs of 360-cameras (epipolar geometry), and detail its practical implementation.

2.1. Theory

2.1.1. Single 360-degree camera

A 360-camera can be modelled as a point in space with an internal orientation described by an orthogonal frame $e_{x,y,z}$ (figure 1b). As the camera estimates the angular position (θ,ϕ) of a world point X relative to itself, but not its distance, world points are only known with respect to their projections $\boldsymbol{\alpha}$ on the unit sphere,

$$\boldsymbol{\alpha} = (\cos\theta\sin\phi,\ \sin\theta\sin\phi,\ \cos\phi). \qquad (2.1)$$

2.1.2. Two 360-degree cameras in stereoscopic set-up

Consider two 360-cameras, C_1 and C_2. We arbitrarily choose the position and orientation of C_1 as the origin and frame of reference of the world. With respect to C_1, C_2 is translated by a vector t, and its internal frame is rotated by three Euler angles $(\psi_x,\ \psi_y,\ \psi_z)$, which can be represented by a 3×3 rotation matrix $\mathbf{R} = \mathbf{R_x}(\psi_x)\cdot\mathbf{R_y}(\psi_y)\cdot\mathbf{R_z}(\psi_z)$ (figure 1b), where $\det(\mathbf{R}) = 1$ and $\mathbf{R}^{-1} = \mathbf{R^T}$. Since there is no intrinsic length scale in this geometry as cameras only evaluate point projections, we set $|t| = 1$, and the correspondence with real-world units can be made by measuring the distance between the two cameras in the experimental set-up.

2.1.3. Triangulation: theory

Given a point X in space, its coordinates are: $X_1 = r_1\boldsymbol{\alpha}_1$ in the frame of C_1, and $X_2 = r_2\boldsymbol{\alpha}_2$ in the frame of C_2. To express X_2 in the frame of C_1, it needs to be rotated back, and therefore has coordinates $\mathbf{R}^{-1}X_2$. From there, we obtain the geometric relation (vector addition),

$$X_1 - (t + \mathbf{R}^{-1}X_2) = 0. \qquad (2.2)$$

As a consequence, vectors X_1, $(\mathbf{R}^{-1}X_2)$, and t are coplanar, and so are their angular projections, such that

$$\boldsymbol{\alpha}_1 \cdot [t \times (\mathbf{R}^{-1}\boldsymbol{\alpha}_2)] = 0. \qquad (2.3)$$

By writing the cross product as a matrix multiplication $t \times v = \mathbf{T_x}v$, we define the fundamental matrix as $\mathbf{F} = \mathbf{T_x}\cdot\mathbf{R}^{-1}$ [24], such that

$$\boldsymbol{\alpha}_1 \cdot (\mathbf{F}\boldsymbol{\alpha}_2) = 0. \qquad (2.4)$$

2.2. Implementation

2.2.1. Camera data

360-cameras have internal or external software that performs the stitching between the FOVs recorded from different objectives. One common output of these stitching procedures is a movie consisting of equirectangular frames of dimension $n_p \times 2n_p$ pixels^2 which map the planar coordinates (x,y) onto the azimuthal angle θ and the polar angle ϕ: $(x,y) \in [\![1, 2n_p]\!] \times [\![1, n_p]\!] \longrightarrow (\theta, \phi) \in [0, 2\pi[\times [0, \pi]$ (figure 1c,d). The angles are obtained using

$$\theta = x \times \frac{2\pi}{2n_p} \qquad (2.5)$$

and

$$\phi = y \times \frac{\pi}{n_p}, \qquad (2.6)$$

and the spherical coordinates $\boldsymbol{\alpha}$ are defined in equation (2.1). The three-dimensional reconstruction from sets of points $\{(\theta,\phi)\}$ in pairs of frames requires three steps: calibration, matching and triangulation, as described in the following sections.

2.2.2. Calibration

Calibration aims to determine the position t and orientation $\mathbf{R}$ of C_2 relative to C_1. We assume that we have a set of N *matched* points between the two cameras. (These can be obtained from an identifiable trajectory, or by using specific points such as the corners of a chessboard, or by manual identification of specific features.) From the set of matched points, we propose two methods to compute $(t,\mathbf{R})$.

Method 1: optimization search. The idea is to find the set of t- and $\mathbf{R}$-coordinates that minimizes the sum of the distances between triangulated points in each camera. Assuming test values $t^\star$ and $\mathbf{R}^\star$, there exists a set of distances r_1, $r_2 \geq 0$ such that $|r_1\boldsymbol{\alpha}_1 - (t^\star + r_2(\mathbf{R}^\star)^{-1}\boldsymbol{\alpha}_2|$ is minimum [24]. The optimization search occurs on a six-dimensional space since $t = (t_x, t_y, t_z)$ and $\mathbf{R}$ is determined by the three Euler angles $\psi_{x,y,z}$, with the additional constraint $t_x^2 + t_y^2 + t_z^2 = 1$. Finally, the problem reads

$$\min_{\substack{\{t_x,t_y,t_z,\psi_x,\psi_y,\psi_z\} \\ t_x^2+t_y^2+t_z^2=1}} \sum_i |r_{1,i}\boldsymbol{\alpha}_{1,i} - (t + r_{2,i}\mathbf{R}^{-1}\boldsymbol{\alpha}_{2,i})|, \qquad (2.7)$$

and can be solved using Matlab's `fmincon` function.

Method 2: fundamental matrix. The camera pose can also be determined from the fundamental matrix, which can be computed using the Matlab built-in function `estimateFundamentalMatrix`. (Note that this function is designed for planar calibration, and therefore it only takes two-dimensional vectors as arguments, assuming that the third coordinate is 1. Consequently, using this function requires renormalizing the projection vectors $\boldsymbol{\alpha}$ by their third coordinate $\tilde{\boldsymbol{\alpha}} = \boldsymbol{\alpha}/\alpha_z$.) From the estimation of $\mathbf{F} = \mathbf{T_x}\cdot\mathbf{R}^{-1}$, t is simply a unitary vector in the null space of $\mathbf{F}^{-1}$, which leaves an ambiguity of factor ±1. Since $\det(\mathbf{T_x}) = 0$, estimating $\mathbf{R}$ relies on singular-value decomposition, for example using the method described in [25]. Each possibility for t contains two possibilities for $\mathbf{R}$, which makes a total of four solutions. Of those, two are improper rotations (determinant −1), which leaves only two possibilities. Choosing the right one may rely on an experimental estimation; for example, it is convenient to arrange the cameras so that $\mathbf{R} \simeq \mathbf{I}$ (identity matrix).

Both methods are susceptible to numerical imprecision. For method 1, optimization search may return a local (rather than global) minimum. For method 2, the fundamental matrix factorization has more than one solution, and singular-value decomposition can have large numerical errors for ill-conditioned matrices. Therefore, we recommend that both methods be employed to verify that they provide consistent results (electronic supplementary material, S6.2). If they do not, where and why they fail should be examined.

2.2.3. Matching

Points extracted from pairs of frames are originally not matched, so a pairing algorithm has to be employed to determine point correspondences. Given t, $\mathbf{R}$, a set of n_1

points $\{\boldsymbol{\alpha}_{1,i}\}$ in C_1, and n_2 points $\{\boldsymbol{\alpha}_{2,j}\}$ in C_2, an optimal pairing can be made by applying the Hungarian algorithm on an appropriate cost matrix $[c_{i,j}]$. We chose the cost of pairing $\boldsymbol{\alpha}_{1,i}$ with $\boldsymbol{\alpha}_{2,j}$ as equal to the smallest possible distance: $c_{i,j} = \min_{r_1, r_2 > 0} |r_1 \boldsymbol{\alpha}_{1,i} - (t + r_2 \mathbf{R}^{-1} \boldsymbol{\alpha}_{2,j})|$.

2.2.4. Triangulation: implementation

Given the camera pose $(t, \mathbf{R})$ and two matched points $\boldsymbol{\alpha}_1$, $\boldsymbol{\alpha}_2$ corresponding to projections of world point X, the distances $r_1, r_2 \geq 0$ from C_1, C_2, respectively, can be calculated by minimizing the distance $|r_1 \boldsymbol{\alpha}_1 - (t + r_2 \mathbf{R}^{-1} \boldsymbol{\alpha}_2)|$ using a linear solver such as Matlab's `lsqnonneg`. From there, $X = r_1 \boldsymbol{\alpha}_1$. Note that triangulation is impossible for points lying on the same line as t.

2.2.5. Tracking

Flash locations in two-dimensional movie frames were extracted by centroid calculation after global thresholding of pixel values. Flash intensity fluctuations were not considered here: fireflies were either 'on' or 'off'. This is justified given the sharp increase and decrease of flash intensity patterns (see [11] and electronic supplementary material, S3.4). Individual three-dimensional points were subsequently concatenated into streaks (spatial localization of a single, continuous flash) and trajectories (sets of consecutive streaks from the same individual), as described in the electronic supplementary material, S5.

3. Experimental set-up

Data collection on the firefly species *P. carolinus* took place in early June 2019 on the Tennessee side of GSMNP per research permit (GRSM-2019-SCI-2075) by the National Park Service. We performed two types of experiments: recordings in the fireflies' natural habitat, and recordings in a controlled environment.

3.1. Equipment

We used two GoPro Fusion cameras as our 360-cameras. Temperature was recorded using two Kestrel temperature data loggers (one reading every 5 min). The cameras were positioned on small tripods (0.6 m above ground), and aligned manually as precisely as possible to have the same side facing the same direction (so that $\mathbf{R}$ is close to identity). The spacing between the two cameras was always set to 3 ft (0.91 m) using a wooden yard stick (figure 2b). We recorded at either 30 or 60 frames per second (fps) and the ISO was manually set to 1600. We applied black electrical tape on the screens and LEDs of the cameras so as not to perturb fireflies with artificial light signals. The recorded footage was then processed using the software provided with the cameras, GoPro Fusion Studio, in order to create equirectangular movies in high-resolution (4K) MPEG format which could later be processed in Matlab (figure 1c,d). It is crucial to render the movies using no stabilization option in order to maintain constant orientation throughout the movie. In order to identify simultaneous frames in both cameras, a brief light signal was triggered a few seconds after recording started. The beginning of the signal marked the frame of reference in each movie, allowing us to estimate the exact delay (within one frame) between cameras. We later found that using cross-correlations

between frames from both cameras resulted in identical delay estimations, and used that to confirm that delays remained constant even after 2 h of recording. Calibration was performed using the trajectory of a small LED. For camera pose estimation, we used the results from the fundamental matrix computation after verifying consistency with the other proposed methods (see electronic supplementary material, S6.2).

3.2. Data collection in natural habitat

The specific GSMNP site for natural habitat recordings was situated between a trail along a creek and a steep ridge, in a bushy area (figure 2a) that had been observed in previous nights to show high activity of *P. carolinus*. Prior to the start of the display (about 30 min before sunset), the two 360-cameras were placed in a small terrain depression clear from trees and close to the bottom of the ridge (figure 2b). They were positioned side by side on firm ground, and facing the same direction (figure 2b). Recording at 30 fps was started using a remote control at 21.15 EST, 29 min after sunset (20.46), and continued for about 90 min. Local ambient temperature was $18.5 \pm 0.5°C$.

3.3. Data collection in controlled environment

In addition to recording firefly displays in the natural, unperturbed habitat, we performed a series of controlled experiments, in which a specific number of *P. carolinus* male fireflies were placed in a large tent. For these experiments, fireflies were gently captured during the peak flashing hour using insect nets, and delicately placed into Petri dishes for up to a few minutes before being introduced into the tent, where they were visually inspected to confirm their sex and species (see electronic supplementary material, S3.1). They were then placed by increasing numbers into a cuboid black fabric tent of dimensions $2\,m \times 1.5\,m \times 1.5\,m$ (*x-y-z*, figure 5b). An additional black plastic tarpaulin was added on top in order to ensure visual insulation from fireflies on the outside. Outside temperature decreased from 19°C to 17°C over the course of the experiments, while the temperature inside the tent was 18°C. Each experiment lasted for 15 min recorded at 60 fps (about 55 000 frames), and consisted of the same stereoscopic set-up (figure 5a).

In the set of experiments presented here, we introduced a single firefly first, and additional fireflies subsequently every 15 min to reach cumulative numbers of $n = 5, 15, 25$ and 40. Due to time constraints and the difficulty of finding fireflies in the tent, we did not attempt to remove fireflies before introducing new ones. All fireflies were released after no more than 2 h, and great care was taken so as not to harm them.

4. Results

4.1. Natural habitat

4.1.1. Spatial distribution of flash occurrences

The three-dimensional reconstruction of flash occurrences in the natural habitat (5 min interval starting at 22.00) shows a *P. carolinus* swarm that closely follows the slope of the surrounding terrain, and notably flashes almost exclusively in a layer of about 2 m above ground (figure 2d–g and electronic supplementary material, movie S2). Viewed from above, the reconstructed swarm reveals the limits of the imaging
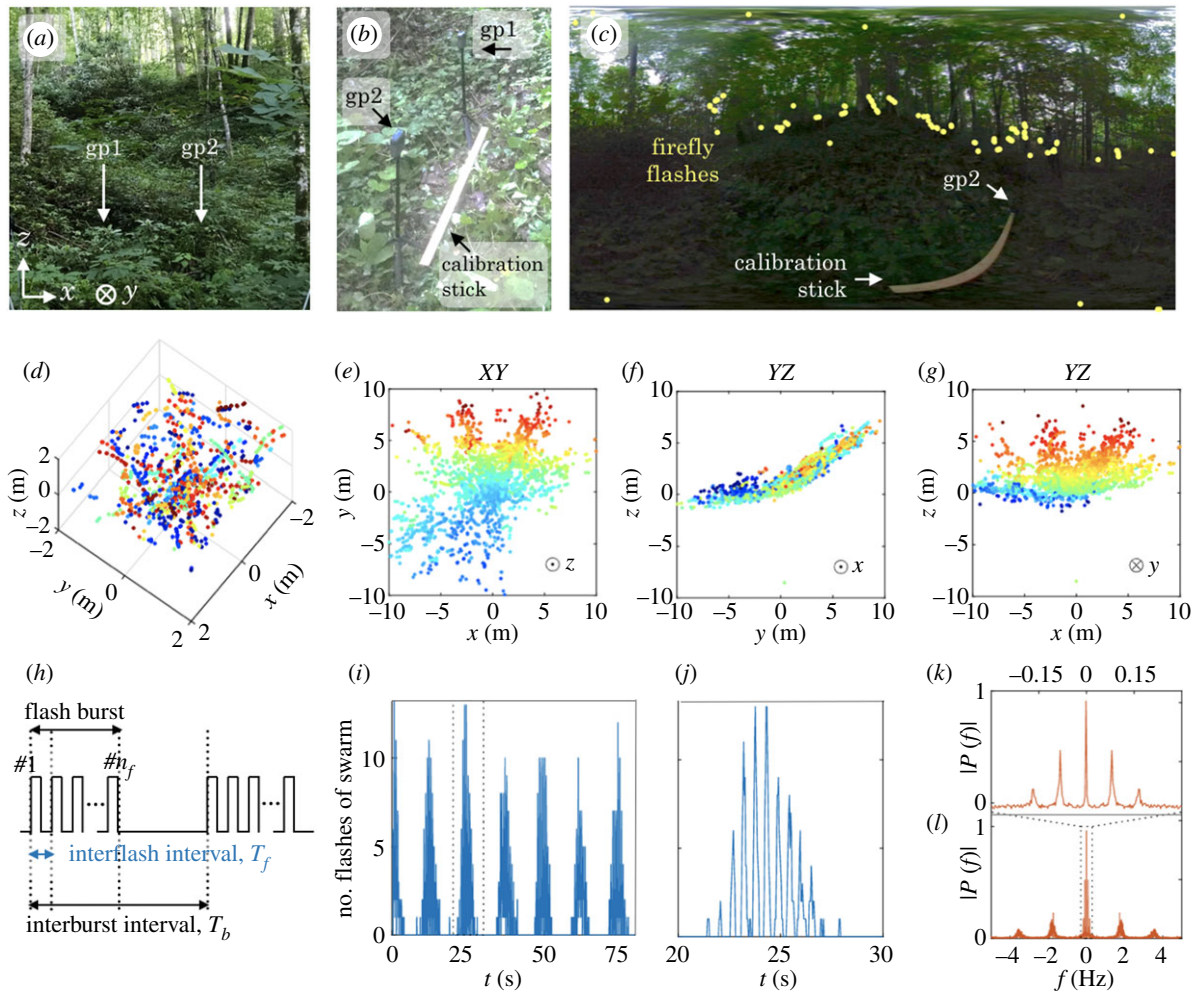
Figure 2. Spatial and temporal patterns in field experiments. (a) Broader view of GoPro surrounding environment. The rising ridge is clearly visible in the distance. The cameras (gp1 and gp2) are situated approximately as indicated, but surrounding vegetation conceals them. The coordinate system is defined in the bottom-left corner, with xy defining the horizontal plane and z the vertical axis. (b) GoPro cameras standing on small tripods and separated by 0.9 m. (c) Contrast-adjusted 360-view from gp1, with yellow dots showing the locations of a few firefly flashes, mostly concentrated along the ground. The yard stick in (b) is also seen, with gp2 standing at the other end. See also electronic supplementary material, movie S1. (d) Three-dimensional reconstruction in a $2 \times 2 \times 2\ \mathrm{m}^3$ cube, centred around gp1. Colours indicate occurrence in time (blue to red), over 5 min. See also electronic supplementary material, movie S2. (e–g) Two-dimensional projections of the full reconstructed swarm, from (e) above, (f) the side and (g) the front. Colours (blue to red) indicate the value along the axis perpendicular to the page (z,x,y, respectively, as indicated in the bottom-right corner of the plots). (h) Schematic of P. carolinus's flash pattern. Flashes are produced in bursts of variable n_f flashes. These bursts are separated by a second time scale, the interburst interval T_b (time from the onset of one flash burst to the onset of a consecutive flash burst). During the time between bursts, no flashes are produced. (i) Time series of the number of flashes per frame over 2 min 30 s. Bursts of collective flashing occur at regular intervals (about 12.5 s). (j) Zoom on the flash burst between $t = 20$ s and $t = 30$s. The burst shows a succession of peaks at regular intervals (about 0.5 s), suggesting synchrony. The characteristic triangular shape of the burst is seen for all bursts. (k,l) Fourier transform of the time series in (i) showing two distinct frequencies. The low frequency in (k), about 0.08 Hz, corresponds to interburst intervals. The high frequency in (l), about 1.75 Hz, corresponds to interflash intervals.

technique: flashes further than about 10 m are not captured, and visual occlusion creates significant 'blind zones'. However, triangulated positions show clear streaks of light (figure 2d). This dataset is available for visualization with FireflyNavigator (electronic supplementary material, S1.2).

4.1.2. Temporal pattern of flash occurrences

In every frame of the movie, zero, one or several flashes are captured. The time series of the number of flashes is presented in figure 2i,j and shows a doubly periodic pattern. Bursts of flashes happen at regular intervals (interburst intervals T_b, figure 2i), with a maximum of about 15 simultaneous flashes recorded, and are separated by periods of absolute darkness. By zooming on these bursts (figure 2j), another temporal pattern appears: bursts consist of a train of a few

flashes, happening synchronously, also at a well-defined interflash interval $T_f \simeq 0.5$ s. The frequency spectrum (Fourier transform) of the flash time series further confirms the regularity of these two processes by revealing pronounced peaks at frequencies $1/T_b = 0.08$ Hz and $1/T_f = 1.75$ Hz (periods of 12.5 s and 0.57 s, respectively; figure 2k,l). The fact that these frequencies appear as sharp peaks in the power spectrum indicates that these two processes occur at well-defined time intervals. These simple quantitative results demonstrate that the flashing display of P. carolinus is synchronous, intermittent and precise, in agreement with previous measurements by Copeland & Moiseff [11,12] which describe similar intermittent (or 'discontinuous') synchrony. However, unlike their previous observations that 'group flashing terminated abruptly' [11], we consistently observed a triangular shape of flash bursts, with a slow
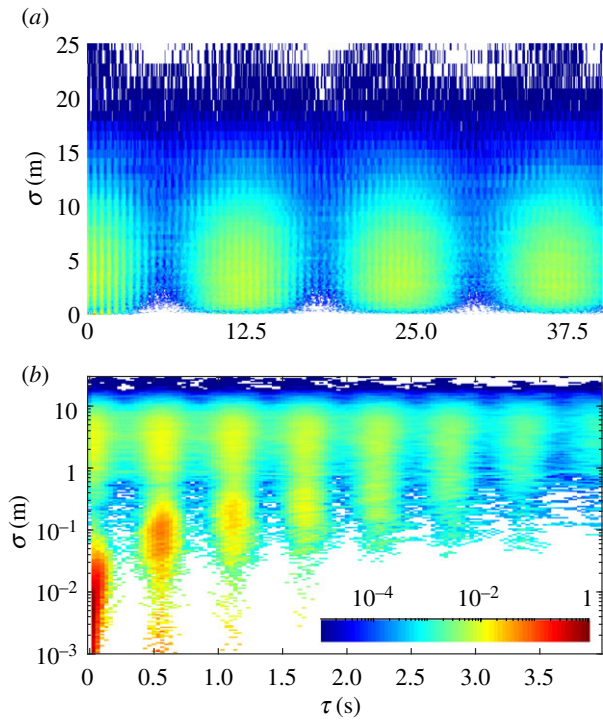
Figure 3. Spatio-temporal correlations: probability distribution functions in the delay-separation (τ, σ) plane. (*a*) Large time and length scales, showing interburst correlations. (*b*) Small time and length scales, showing intraburst correlations.

fading-out phase over a few beats (figure 2*j*). This triangular pattern might suggest some underlying propagation of information within the swarm (electronic supplementary material, S4), and is therefore an important feature of collective flashing. In controlled experiments described below, we show that this shape is not an experimental artefact.

4.1.3. Spatio-temporal correlations of flash occurrences

These results demonstrate that a swarm of *P. carolinus* males is a strongly correlated system. The mechanisms underlying their collective behaviour, such as information propagation, can be uncovered by the study of spatio-temporal correlations. For each recorded flash occurrence, we associate a time t_i and a three-dimensional position x_i. Then, for every pair of flash occurrences (i,j), we calculate the separation $\sigma_{ij} = |x_j - x_i|$ and the delay $\tau_{ij} = |t_j - t_i|$, and we consider the distribution of σ versus τ in figure 3. The probability density is displayed by colour using a logarithmic scale, and the smallest increment for τ is one frame (0.033 s). The temporal structure of flash occurrences, as reported in figure 2, is reflected in this distribution: correlated peaks occur every 12.5 s (figure 3*a*), corresponding to flash bursts, and each of them consists of a series of high and low fringes every 0.55 s (figure 3*b*), corresponding to interflash intervals. Spatial correlations between bursts in figure 3*a* extend across the entire swarm (peak in the 0–10 m range), demonstrating that flash bursts span the entire (recorded) swarm. Spatial correlations at short times (figure 3*b*) exhibit a bimodal distribution along the σ-axis. The peaks at small σ correspond predominantly to correlations within a streak ($\tau \leq 0.1$ s) and between successive streaks from the same firefly ($\tau = 0.55, 1.10, 1.65, \ldots$ s). The peaks in the 1–10 m range, at all delays including $\tau = 0$ s, are more significant, and suggest that there is no characteristic time scale for information propagation, at least at resolvable times. This

important result, which will be investigated in more depth in future work, could be well explained by the following hypothesis: due to significant visual occlusion, and a mixture of fireflies at rest and moving, it is possible that information transfer relies on a network of visual connectivities with no well-defined length scale. Two fireflies at short distance might not be able to interact due to visual occlusions, but two fireflies far apart could if connected by a line of sight.

4.1.4. Flight kinematics

Three-dimensional reconstruction also provides insights into the kinematics of moving fireflies. The analysis of individual streaks (flashes spanning at least four consecutive frames) shows a wide range of firefly motilities. Streak velocities v show a continuum between immobility and fast flights at speeds up to 30 cm s^{-1} (figure 4*a*; the distribution reported here is expected to contain artefacts as flying flashers are more likely to be recorded than immobile ones, which suffer from greater visual occlusion). Comparable, but usually larger, velocities have been observed in other insect flights [26,27]. Streak curvature radii r_c are also widespread, revealing sharp turns as well as straight flights (figure 4*b*). Streak accelerations, calculated as $a = v^2/r_c$, span two orders of magnitude, with an upper limit comparable to the Earth's gravity (figure 4*c*), analogous to what has been seen in other insects [26]. Interestingly, the distribution of r_c versus v shows two well-defined limiting branches (figure 4*d*). The lower branch (large v, small r_c) marks the 'high-acceleration' regime, corresponding to sharp and fast turns. The upper branch is more surprising, and suggests that slow and straight trajectories are not possible per firefly propulsion.

Next, we report observations pertaining to long recorded trajectories (longer than 2 s), typically consisting of at least four streaks. These trajectories show a diversity of patterns. Considering the horizontal excursion δr_{xy} between the trajectories' end-points, we observe in figure 4*e* a continuum between trajectories which are almost stationary, and others that cover up to 1 m. The vertical excursion δz is asymmetrically distributed (figure 4*f*), with downward trajectories typically extending further. Trajectories appear to be never completely vertical (large $|\delta z|$, small δr_{xy}) but sometimes completely horizontal (figure 4*h*), which potentially suggests limitations of flight capabilities. Furthermore, the ratio of a trajectory's path length s to its end-to-end distance $\delta r = \sqrt{\delta r_{xy}^2 + \delta z^2}$ (figure 4*g*) shows that, while most trajectories are rather straight ($s/\delta r \simeq 1$), a significant fraction seem very curved and loopy (large $s/\delta r$).

For illustration, we present a few trajectories corresponding to these different cases: large horizontal excursions (figure 4, row *h*), large downward displacements (row *i*) and highly curved (row *j*). These trajectories are shown in boxes of (1 m)^3 (rows *h, i*) or (0.5 m)^3 (row *j*) for scale. These different types of trajectories may be hypothesized to correspond to different stereotyped behaviours. For example, long and downward trajectories have been observed in male fireflies courting a responding female near the ground [28]. Large horizontal excursions might correspond to exploratory phases.

4.2. Controlled environment

A known number of *P. carolinus* males were placed in a tent in order to study flashing interactions among a small number of fireflies.
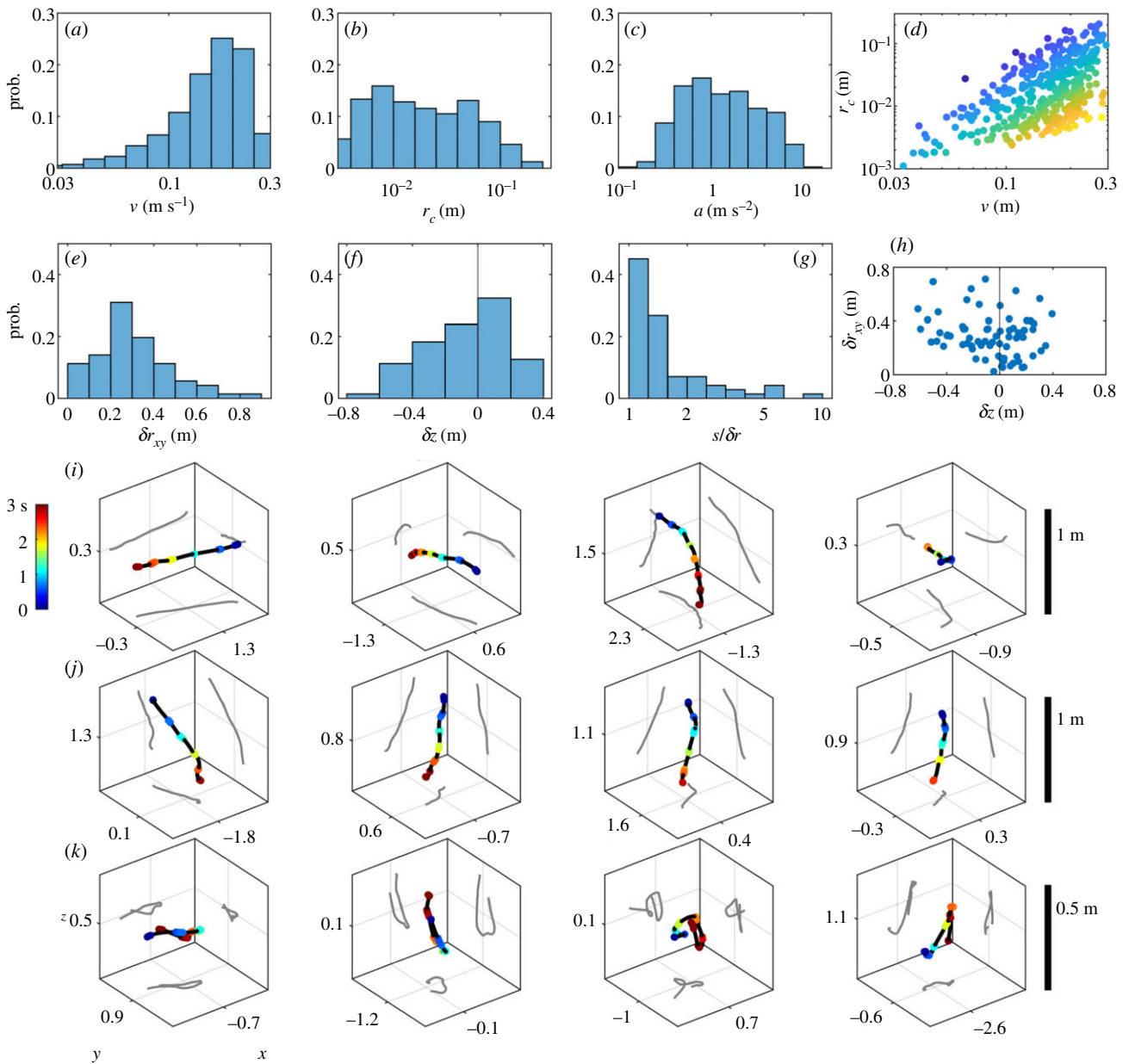
Figure 4. Kinematics of natural flights. (*a*–*c*) Distributions of (*a*) streak velocity *v* (mean frame-to-frame displacement), (*b*) radius of curvature r_c (circle fit to streak positions) and (*c*) acceleration $a = v^2/r_c$ for naturally occurring firefly flashes. (*d*) Scatter plot of r_c versus *v*, with colours indicating *a* value (blue to yellow). Accessible kinematics span only a portion of the plane; notably, the high-acceleration regime (bottom-right; fast and curved streaks), and the slow straight regime (top-left) are excluded. (*e*–*g*) Trajectory (ensemble of streaks belonging to the same firefly) metrics: distributions of (*e*) horizontal displacements δr_{xy}, (*f*) vertical displacements δz and (*g*) trajectory length *s* over end-to-end distance δr. (*h*) Scatter plot of horizontal displacements versus vertical displacements. (*i*–*k*) Representative trajectories for three different regimes: row (*i*) large horizontal displacements, row (*j*) large vertical displacements and row (*k*) long trajectories with close end-points. Coloured points indicate recorded (triangulated) flashes, and black lines interpolated paths. Rows (*i*) and (*j*) show cubes of $1 \times 1 \times 1\,\mathrm{m}^3$, and row (*k*) $0.5 \times 0.5 \times 0.5\,\mathrm{m}^3$, for scale, with axis values indicating mean position with respect to gp1.

4.2.1. Three-dimensional reconstruction

The three-dimensional reconstruction of flash occurrences in the tent over 15 min at $n = 40$ is shown in figure 5*c*. Aside from a small fraction of points (about 1%) which were localized far above the others and were removed from the figure (see discussion in the electronic supplementary material, S6.2), the triangulated points define a volume which closely resembles the tent's geometry. In particular, dimensions are consistent, and the outline of the curved roof appears clearly (the roof's fabric curves under its weight, figure 5*b*), with a concentration of points at the edges. In accordance with visual observations when emptying the tent at the end of experiments, fireflies tend to stand on the roof and walls, and hide in the edges and corners, especially in the sharp angles at the junction between the roof and the walls.

Although the confining conditions of the tent plausibly perturbed natural behaviour to some extent, the accessible volume was large enough (approx. $4\,\mathrm{m}^3$) that fireflies were able to move and fly freely, as seen in the trajectories in figure 6*c*1–4. This dataset is available for visualization with FireflyNavigator (electronic supplementary material, S1.2).

4.2.2. One firefly

When a single male firefly was introduced in the tent, it emitted flashes continuously over the 15 min of the experiment (figure 6*a*1), even in the absence of a responding female. Flashes lasted typically between 0.10 s and 0.15 s (5–10 frames), although shorter and longer flashes were also recorded (figure 7*a*). (For high-resolution measurements of
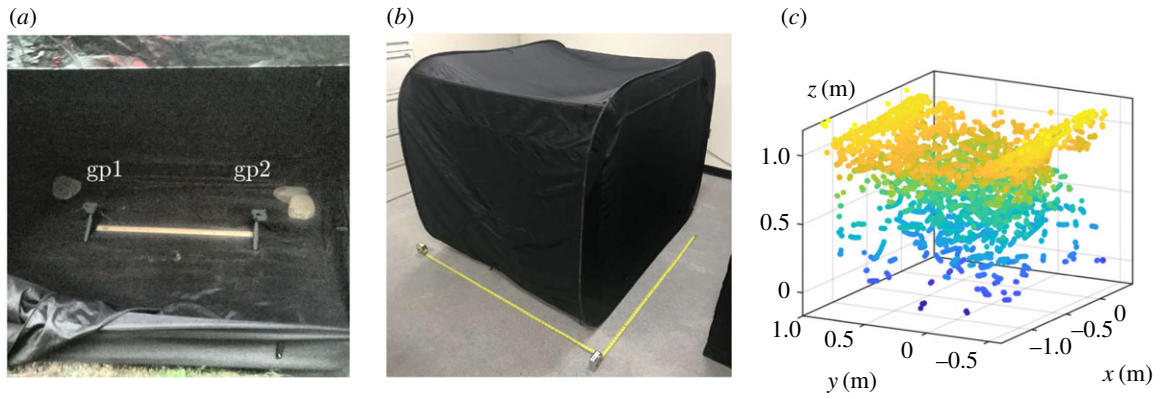
Figure 5. Controlled experiments in a confining tent. (*a*) GoPro cameras inside the tent, separated by the yard stick (0.9 m). (*b*) Tent geometry. The yellow tape measure indicates 1.5 m. The *x*-side on the right is about 2 m long, and contains the zipper opening seen in (*a*). The *y*-side and *z*-side (vertical) are about 1.5 m long. Note the roof fabric curves under its own weight. (*c*) Three-dimensional reconstruction of flash occurrences in the tent (colours indicate height, from blue to yellow). The dimensions of the enclosing volume match tightly those of the tent, and the shape of the top layer mirrors the curvature of the tent's roof.
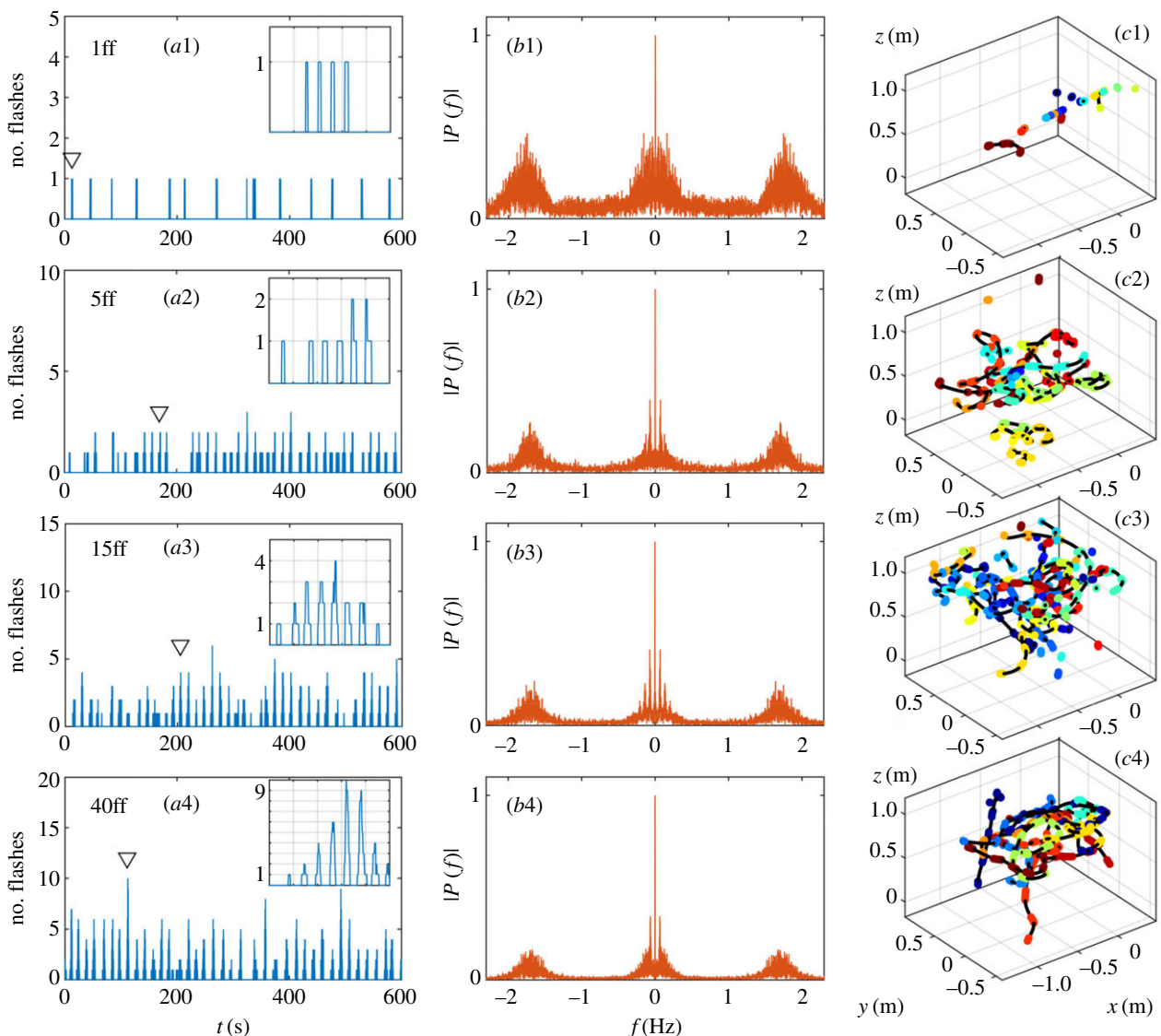

Figure 6. Emergence of collective behaviour in controlled experiments. (*a*1–*a*4) Time series of the number of flash occurrences over 10 min recorded in the tent containing 1, 5, 15 and 40 fireflies, respectively. Insets: close-up of single bursts (over 5 s) indicated by downward triangles. (*b*1–*b*4) Corresponding frequency power spectra |*P*(*f*)| (Fourier transforms), showing the interflash frequency at 1.75 Hz and the emergence of a burst frequency at 0.08 Hz when several fireflies interact. (*c*1–*c*4) Example trajectories (longest flights) for corresponding confined fireflies. Colours indicate time over 15 min (blue to red).

the quasi-rectangular intensity shape of a single flash, see [11].) Flashes occurred by bursts of typically four consecutive flashes, and overall between one and six (figure 7*b*), and,

independently of the pattern, the time interval between two successive flashes was sharply distributed around 0.45 s (25–30 frames), as evidenced in both the distribution of
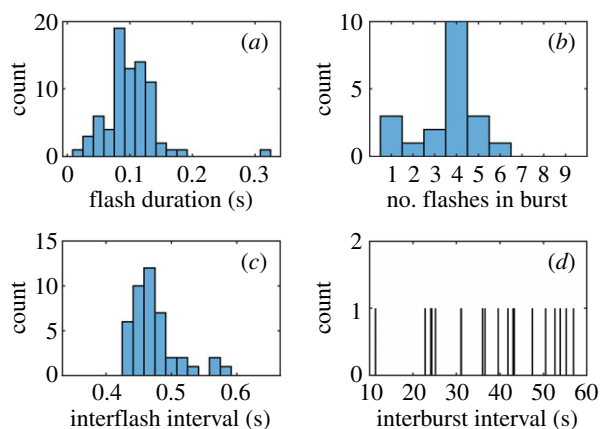
Figure 7. Statistics of a single firefly's flash pattern, recorded at 60 fps. (*a*) Distribution of flash durations. Most flashes last between 5 and 10 frames (0.08–0.16 s). (*b*) Distribution of number of flashes per burst. A typical burst consists of four flashes, although shorter or longer ones are also common. (*c*) Distribution of interflash intervals. Flash intervals appear as very regular, at 0.45 ± 0.05 s. (*d*) Distribution of time intervals between successive bursts. There seems to be no characteristic time between two bursts, unlike what is observed in collective flashing.

interflash intervals (figure 7*c*) and the 1.75 Hz peak in the frequency spectrum (figure 6*b*1). Flashing occurred while both flying or standing on the tent's structure (figure 6*c*1). These observations are generally consistent with previous studies of *P. carolinus* flash patterns [11,12]. Most importantly, unlike interflash intervals, time intervals between successive bursts did not show any regularity, spanning a wide range from 12 s to 1 min (figure 7*d*). Similar findings occurred in repeated experiments (see electronic supplementary material, S3.2).

4.2.3. Five fireflies

Four fireflies were subsequently introduced to bring the total to *n* = 5. Flashing continued throughout the experiment, with many flights recorded (figure 6*a*2,*c*2). It appears that fireflies attempted to synchronize their flash signals, as evidenced by the temporal distribution of flash occurrences. Indeed, the majority of flash bursts comprised at least two simultaneously active fireflies, whose flashes occurred synchronously (figure 6*a*2). Trajectory identification, enabled by the spatial localization of flash streaks, provides further insights into the onset of collective synchrony. Figure 8 shows that the firefly that initiates a burst tends to flash the longest, and that followers start their own flashes *already synchronized*. This strongly contrasts with common mathematical models which describe the onset of synchrony in coupled oscillators through a distribution of phases that becomes continuously sharper over time [14,15]. Followers can either stop before the flashing leader (figure 8*b*) or continue after him (figure 8*a*), which suggests that flashing information could be transferred in a relay-like manner throughout large swarms. Finally, while flashing bursts seem aperiodic (e.g. large gap at *t* = 200 s in figure 6*a*2), the emergence of a peak at low frequencies (figure 6*b*2) hints at some regularity in the collective flashing pattern.

4.2.4. Fifteen fireflies

This regularity becomes more pronounced at *n* = 15, where bursts occur periodically in the time series (figure 6*a*3) and prominent peaks (and their harmonics) emerge in the frequency spectrum
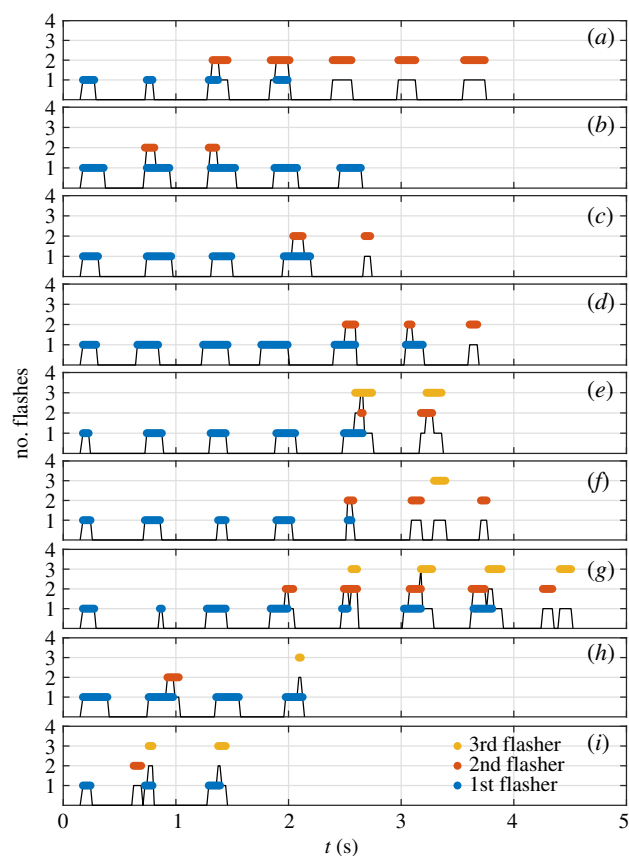

Figure 8. Patterns of synchronous collective flashing. The black line indicates the number of flashes at a given time. The coloured segments indicate flashes coming from the same firefly. In panel (*a*), for example, one firefly starts flashing, and repeats three more times (blue). A second firefly starts on the third beat, and continues for a total of five flashes. It is slightly delayed on the third beat, but starts first on the fourth. In panel (*e*), a second and third firefly start together (although slightly late) on the fifth flash.

at $1/T_b = 0.08$ Hz (figure 6*b*3). This interburst frequency is identical to the one measured in the wild, and was absent in the flash pattern of a single firefly. Therefore, this suggests that occurrence of a well-defined interburst interval is an emergent property of collective behaviour. The interflash interval at 1.75 Hz remains similar to that of a single firefly (figure 6*b*3).

A second important observation concerns the collective kinematics during a burst. In most bursts, only one firefly is seen flying, while others are standing or walking (figure 9; electronic supplementary material, S3.3 and movie S3). The flying trajectory typically starts the earliest, and comprises the most flashes. This observation could be related to a mechanism which optimizes information transfer while conserving the group's collective energy resources. Alternatively, it could reveal behavioural differentiation. It was not possible to determine whether it is always the same firefly that is flying in different bursts, as too much localization information is lost in the few seconds of darkness between bursts.

4.2.5. Forty fireflies

The flashing dynamics at 40 fireflies is qualitatively similar to the 15-firefly case, but the larger number of flashes provides more accurate observations. Flashes occur during bursts regularly spread in time; each burst consists of a few synchronous flashes, and presents the same triangular shape as observed in the wild, wherein the number of flashes slowly increases, reaches a maximum and then slowly decreases (figure 6*a*4).
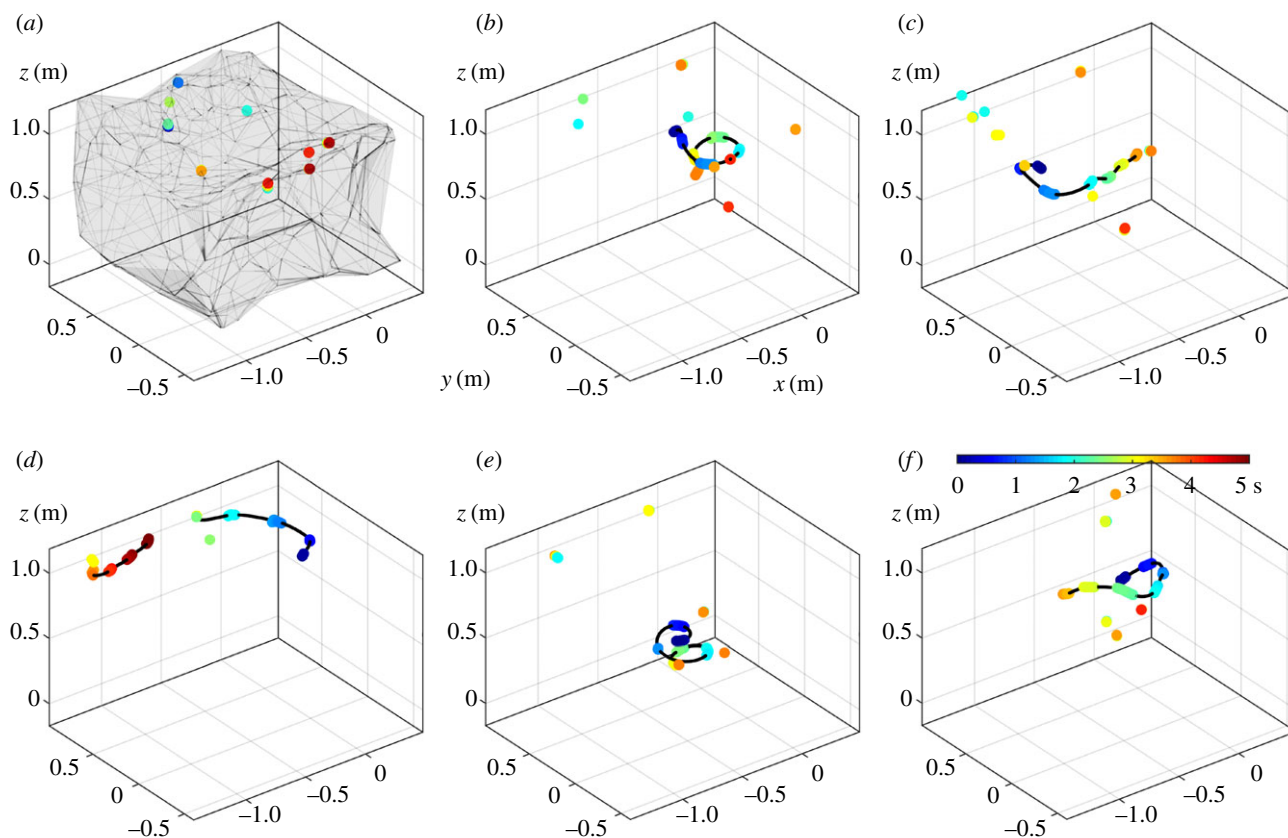
Figure 9. (a–f) Firefly trajectories during flash bursts. Coloured dots indicate recorded flash occurrences over a time window of 5 s (blue to red), and black lines indicate interpolated flight paths. The grey volume in the first plot represents the approximate tent outline obtained from all flash positions (alpha shape), for reference. All six plots have the same scale and position. While many flashes occur during a burst, most of them come from immobile fireflies, usually standing on the tent's ceiling or walls. See also electronic supplementary material, S3.3 and movie S3.

This pattern can easily be considered as the extension of the pair synchronization presented with five fireflies to the case of many fireflies (electronic supplementary material, S4).

In summary, these controlled experiments at increasing density of fireflies show that the synchronous, intermittent flashing display of *P. carolinus* in the wild is the result of individual and collective behaviours. While the interflash interval at 1.75 Hz is identical for a single firefly or a group of fireflies, the emergence of a well-defined interburst interval necessitates a plurality of individuals. Burst periodicity starts when about 15 males are allowed to interact, a number similar to what was found in previous studies as a threshold for collective behaviour [29]. Each burst consists of a few synchronous flashes, and exhibits a triangular shape (slowly increasing then slowly decreasing number of active fireflies) similar to that observed in the wild, hence confirming that these observations in the wild are true and not the result of experimental artefacts such as limited depth of field. While many fireflies flash in unison during a burst, only a few are flying, while others appear immobile or slowly walking. Finally, male collective display occurs even in the absence of a responding female flash, at least over the course of 15 min.

5. Method limitations and applications

5.1. Technique validation and limitations

The three-dimensional reconstruction of firefly flashes using pairs of 360-cameras, reported here for the first time (to the best of our knowledge), appears to be generally very reliable and accurate. Reconstructed swarms in the wild follow precisely the geometry of the surrounding terrain (figure 2). Recordings in controlled experiments also faithfully reproduce the shape of the confining tent (figure 5). Spatial streaks and trajectories often exhibit a resolution better than 1 cm, as seen in previous figures and accessible to the reader in our interactive FireflyNavigator (electronic supplementary material, S1.2). As with any experimental technique, however, this method has limitations which ought to be acknowledged. We discuss briefly the most significant ones here.

5.1.1. Artefacts in 360-degree movies

First, recording over an entire sphere necessarily requires stitching different FOVs together. While this is usually performed by commercial software, small stitching discrepancies are known to be largely unavoidable, creating localization 'jumps' along FOV edges in rectangular frames. 360-cameras built around more than two lenses might provide better stitching. Second, projecting a sphere onto a plane generates stereographic distortions, so that objects near the poles are stretched out and localized with less accuracy. The GoPro Fusion Studio software, however, enables changing the orientation of the projection, so that, if important dynamics occur near the pole of a movie, the axes' origin can be modified to place these events at the equator.

5.1.2. Triangulation resolution

The finite resolution on angle estimation in equirectangular frames implies that triangulation becomes less precise with increasing distance and along the cameras' connecting line.

We discuss theoretical limits to resolution in more detail in the electronic supplementary material, S6.1. Briefly, assuming a localization precision of 1 pixel in the equirectangular projection, and given that a frame contains over 3000 horizontal pixels in our movies (spanning 2π rad), the resolution on azimuthal angles θ_1, θ_2 is $\hat{\delta\theta} \sim 10^{-3}$ rad. From geometrical considerations, the error on the distance r_1 to camera C_1, $\hat{\delta r_1}$, can be related to $\hat{\delta\theta}$ through

$$\hat{\delta r_1} = A(\theta_1, \theta_2)\, \hat{\delta\theta}, \qquad (5.1)$$

where $A(\theta_1, \theta_2) > 0$ spans several orders of magnitude, and depends on the distance between the two cameras. For our experimental set-up, we find that the theoretical triangulation resolution is as low as 1 mm in the 1 m radius sphere between the two cameras, and remains below 1 cm in a 3 m radius lobe in front of the cameras. Excluding the zones close to the cameras' connecting line, the theoretical resolution is below 10 cm up to 8 m away. Increasing the distance between cameras would increase accuracy at large distances, but in a visually occluded environment it would also decrease the likelihood of capturing a same flash in both cameras. Other sources of tracking error, such as static localization error (point-spread function), motion blur, the cameras' asynchrony (up to half a frame's duration, about 0.01 s) due to the absence of an external trigger, etc., should be acknowledged, but in practice they are largely negligible, in particular because flashes are small, sparse and slow-moving.

5.1.3. Reconstruction results

Regarding our results of stereoscopic reconstructions, we briefly mention the following observations. First, camera pose $(t, \mathbf{R})$ estimations appear very robust across different numerical methods, with discrepancies below 10^{-2} (electronic supplementary material, S6.2). Second, in our swarm reconstructions, about 1% of triangulated points are clear outliers or fall out of physical range, for example, far outside the tent volume in our controlled experiments (electronic supplementary material, S6.2). This may be due to improper pairing, or rare occurrences in which two flashes from different sources appear at locations that are compatible in terms of triangulation. Similar problems occur with regular stereoscopic vision, and are better addressed through post-processing filtering.

5.2. Firefly density estimations

While firefly activity shows variability between successive years due to a variety of factors, most notably temperature and humidity conditions, it is widely suspected that firefly populations are generally declining [30]. Climate change, habitat loss, increasing light pollution and degrading environment are some of the most probable causes. Therefore, estimating firefly densities is fundamental to understanding firefly resilience and promoting conservation efforts [30]. The use of stereoscopic 360-camera set-ups to record flashing displays is accurate, simple and inexpensive, and therefore may be appropriate for large-scale monitoring programmes. Here, we briefly discuss how three-dimensional reconstructed data could be used to estimate firefly density. The goal is to estimate the number $N(d)$ of flashes recorded within a certain distance d from the midpoint between the two cameras ($t/2$). If fireflies were homogeneously spread out in space, $N(d)$ would grow as d^3. However, for *P. carolinus* at least, we have shown in figure 2f that fireflies stay mostly near the ground (a surface),
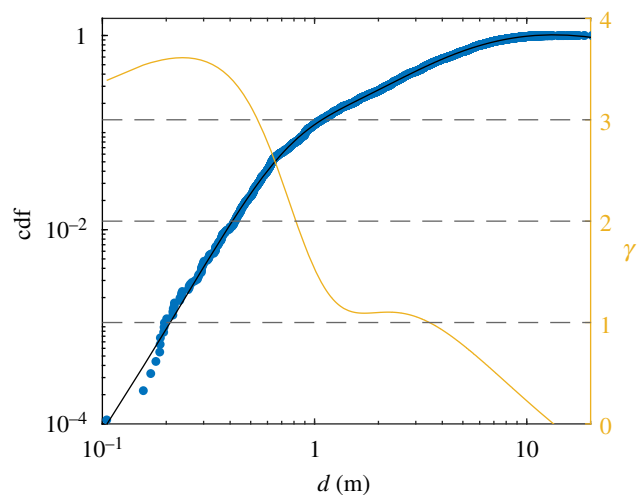

Figure 10. Cumulative distribution function (cdf $= N(d)/N_{\text{total}}$) of the number of recorded flashes within a distance d from the cameras' midpoint, in log–log scale. In order to approximate local values of the slope, i.e. the scaling exponent γ, a fit of the empirical curve (rational function) was performed (black line), and its derivative is plotted in orange on the right axis.

so that $N(d)$ should actually be expected to increase as d^2. That would be accurate under the ideal conditions of a perfectly sensitive camera and a bare environment, but in reality the cameras' limited light sensitivity and visual occlusion from vegetation significantly reduce the number of flashes that can be detected at large distances. Consequently, we expect $N(d)$ to grow as d^γ, with the scaling exponent $\gamma < 2$. In figure 10, we present the cumulative distribution $N(d)/N_{\text{total}}$ as a function of d in a log–log plot, and focus on the local slope which indicates the value of the scaling exponent $\gamma = \partial \log(N)/\partial \log(d)$. We find that for $d < 1$ m, $\gamma \simeq 3$, which is consistent with the fact that the considered volume lies within the 2 m layer above ground in which fireflies swarm. For $d > 10$ m, $\gamma \simeq 0$ as such distances are beyond the cameras' light limitations. But for d between 1 m and 10 m, the scaling exponent is smaller than 2, and closer to 1, indeed reflecting the effect of visual occlusion as discussed above. While it is beyond the scope of this article to propose a complete framework to estimate firefly densities from three-dimensional reconstructed swarms, the plot in figure 10 could serve to establish a calibration curve to extrapolate large-scale densities from local and imperfect measurements.

6. Discussion

By using pairs of 360-cameras in a stereoscopic set-up, we were able to capture the flashing display of *P. carolinus* from within the swarm in a densely forested and visually occluded environment. Triangulation of flash occurrences permitted the three-dimensional reconstruction of mating swarms with sub-centimetric precision within a few metres from the cameras, and hence the identification of specific trajectories consisting of several flashes. A systematic classification of firefly trajectories using statistical methods could provide a basis for the quantitative modelling of behaviour [31]. Our recordings in the fireflies' natural habitat were complemented by controlled experiments in which a small number of *P. carolinus* males were introduced in a large tent (large enough to allow flying) in order to study interactions between a small number of flashers. Our results in the wild extended prior studies of

the intermittent synchrony of *P. carolinus*, and provided additional results relative to the kinematics of firefly trajectories, showing notably different stereotypical flight patterns. Spatio-temporal correlations reflect the flash-burst mechanism of display, and further indicate that instantaneous correlations span several metres, suggesting long-range interactions or a mixture of length scales. Our most surprising findings come from controlled experiments. We showed that while a single, isolated firefly flashes with a regular interflash interval, its bursts have no periodicity. Only when several fireflies are allowed to interact does a well-defined interburst frequency appear, which suggests that intermittent synchrony is an emergent property of collective behaviour. Controlled experiments also tend to show a differentiation between early and mobile flashers, and immobile followers.

These experimental results will inform future mathematical models that account for species-specific discontinuous flash patterns, long-range spatial correlations and spatial mixing due to movement of individuals within the swarm. In the meantime, the low cost and implementation simplicity of the three-dimensional reconstruction technique presented here could foster its deployment for large-scale studies of firefly patterns and monitoring programmes of firefly populations.

References

1. Lewis S. 2016 *Silent sparks: the wondrous world of fireflies*. Princeton, NJ: Princeton University Press.

2. Lewis SM, Cratsley CK. 2008 Flash signal evolution, mate choice, and predation in fireflies. *Annu. Rev. Entomol.* **53**, 293–321. (doi:10.1146/annurev.ento.53.103106.093346)

3. Butail S, Manoukis N, Diallo M, Ribeiro JM, Lehmann T, Paley DA. 2012 Reconstructing the flight kinematics of swarming and mating in wild mosquitoes. *J. R. Soc. Interface* **9**, 2624–2638. (doi:10.1098/rsif.2012.0150)

4. Kelley DH, Ouellette NT. 2013 Emergent dynamics of laboratory insect swarms. *Sci. Rep.* **3**, 1073. (doi:10.1038/srep01073)

5. Stanger-Hall KF, Lloyd JE. 2015 Flash signal evolution in photinus fireflies: character displacement and signal exploitation in a visual communication system. *Evolution* **69**, 666–682. (doi:10.1111/evo.12606)

6. Robertson HA, Carlson AD. 1976 Octopamine: presence in firefly lantern suggests a transmitter role. *J. Exp. Zool.* **195**, 159–164. (doi:10.1002/jez.1401950116)

7. Buck J. 1988 Synchronous rhythmic flashing of fireflies. II. *Q. Rev. Biol.* **63**, 265–289. (doi:10.1086/415929)

8. Buck J, Buck E. 1966 Biology of synchronous flashing of fireflies. *Nature* **211**, 562–564. (doi:10.1038/211562a0)

9. Buck J, Buck E. 1968 Mechanism of rhythmic synchronous flashing of fireflies. *Science* **159**, 1319–1327. (doi:10.1126/science.159.3821.1319)

10. Faust LF. 2010 Natural history and flash repertoire of the synchronous firefly *Photinus carolinus* (Coleoptera: Lampyridae) in the Great Smoky Mountains National Park. *Florida Entomol.* **93**, 208–217. (doi:10.1653/024.093.0210)

11. Copeland J, Moiseff A. 1994 The occurrence of synchrony in the North American firefly *Photinus carolinus* (Coleoptera: Lampyridae). *J. Insect Behav.* **8**, 381–394. (doi:10.1007/BF01989366)

12. Moiseff A, Copeland J. 1994 Mechanisms of synchrony in the North American firefly *Photinus carolinus* (Coleoptera: Lampyridae). *J. Insect Behav.* **8**, 395–407. (doi:10.1007/BF01989367)

13. Moiseff A, Copeland J. 2010 Firefly synchrony: a behavioral strategy to minimize visual clutter. *Science* **329**, 181–181. (doi:10.1126/science.1190421)

14. Ermentrout B. 1991 An adaptive model for synchrony in the firefly *Pteroptyx malaccae*. *J. Math. Biol.* **29**, 571–585. (doi:10.1007/BF00164052)

15. O'Keeffe KP, Hong H, Strogatz SH. 2017 Oscillators that sync and swarm. *Nat. Commun.* **8**, 1504. (doi:10.1038/s41467-017-01190-3)

16. Cavagna A, Conti D, Creato C, Del Castello L, Giardina I, Grigera TS, Melillo S, Parisi L, Viale M. 2017 Dynamic scaling in natural swarms. *Nat. Phys.* **13**, 914–918. (doi:10.1038/nphys4153)

17. Puckett JG, Ni R, Ouellette NT. 2015 Time-frequency analysis reveals pairwise interactions in insect swarms. *Phys. Rev. Lett.* **114**, 258103. (doi:10.1103/PhysRevLett.114.258103)

18. Attanasi A *et al.* 2014 Information transfer and behavioural inertia in starling flocks. *Nat. Phys.* **10**, 691–696. (doi:10.1038/nphys3035)

19. Ballerini M *et al.* 2008 Interaction ruling animal collective behavior depends on topological rather than metric distance: evidence from a field study. *Proc. Natl Acad. Sci. USA* **105**, 1232–1237. (doi:10.1073/pnas.0711437105)

20. Bialek W, Cavagna A, Giardina I, Mora T, Silvestri E, Viale M, Walczak AM. 2012 Statistical mechanics for natural flocks of birds. *Proc. Natl Acad. Sci. USA* **109**, 4786–4791. (doi:10.1073/pnas.1118633109)

21. Cavagna A, Cimarelli A, Giardina I, Parisi G, Santagati R, Stefanini F, Viale M. 2010 Scale-free correlations in starling flocks. *Proc. Natl Acad. Sci. USA* **107**, 11 865–11 870. (doi:10.1073/pnas.1005766107)

22. Ling H, McIvor GE, Westley J, van der Vaart K, Yin J, Vaughan RT, Thornton A, Ouellette NT. 2019 Collective turns in jackdaw flocks: kinematics and information transfer. *J. R. Soc. Interface* **16**, 20190450. (doi:10.1098/rsif.2019.0450)

23. Ling H, McIvor GE, van der Vaart K, Vaughan RT, Thornton A, Ouellette NT. 2019 Local interactions and their group-level consequences in flocking jackdaws. *Proc. R. Soc. B* **286**, 20190865. (doi:10.1098/rspb.2019.0865)

24. Ma C, Shi L, Huang H, Yan M. 2015 3d reconstruction from full-view fisheye camera. (http://arxiv.org/abs/1506.06273)

25. Camera computation and the essential matrix. See http://www.maths.lth.se/matematiklth/personal/calle/datorseende13/notes/forelas6.pdf (accessed 30 February 2020).

26. Wakeling JM, Ellington CP. 1997 Dragonfly flight. II. Velocities, accelerations and kinematics of flapping flight. *J. Exp. Biol.* **200**, 557–582.

27. Wang H, Ando N, Kanzaki R. 2008 Active control of free flight manoeuvres in a hawkmoth, *Agrius convolvuli*. *J. Exp. Biol.* **211**, 423–432. (doi:10.1242/jeb.011791)

28. Case JF. 1980 Courting behavior in a synchronously flashing, aggregative firefly, *Pteroptyx tener*. *Biol. Bull.* **159**, 613–625. (doi:10.2307/1540827)

29. Puckett JG, Ouellette NT. 2014 Determining asymptotically large population sizes in insect swarms. *J. R. Soc. Interface* **11**, 20140710. (doi:10.1098/rsif.2014.0710)

30. Lewis SM *et al.* 2020 A global perspective on firefly extinction threats. *BioScience* **70**, 157–167. (doi:10.1093/biosci/biz157)

31. Berman GJ, Choi DM, Bialek W, Shaevitz JW. 2014 Mapping the stereotyped behaviour of freely moving fruit flies. *J. R. Soc. Interface* **11**, 20140672. (doi:10.1098/rsif.2014.0672)